Characterization of the Pore Structure of the Wulalik Shale in the Majiatan Area of the Ordos Basin

Xi Li[1,2,a], Wenyi Sun[3,*], Weiwei Yang[1,2,b], Junxiang Nan[1,2, c]

[1]National Engineering Laboratory for Exploration and Development of Low-Permeability Oil & Gas Fields, Xi'an, 710018, Shaanxi, China
[2]Research Institute of Exploration and Development, PetroChina Changqing Oilfield Company, Xi'an, 710018, Shaanxi, China
[3]State Key Laboratory of Continental Dynamics, Department of Geology, Northwest University, Xi'an, 710069, Shaanxi, China

[a]lixi2_cq@petrochina.com.cn,[*]sun_wenyi@stumail.nwu.edu.cn
[b]yww1_cq@petrochina.com.cn, [c]njx_cq@petrochina.com.cn

Abstract. Analyzing the nanopore structure of organic matter-rich shale is the basis for evaluating shale reservoir properties and the potential for shale gas resource exploration and development. In this paper, we evaluate the pore characteristics and connectivity of the shale of the Lower Paleozoic Ordovician Wulalik Formation at the western margin of the Ordos Basin by field-emission scanning electron microscopy, micrometer CT and three-dimensional reconstruction techniques: (1) Micron CT can show the three-dimensional spatial structure of shale pores, which is more conducive to characterizing shale pores in combination with other experimental methods; (2)The marine shale of Ordos Basin Western Ordovician Wulalik Formation is more developed in overall porosity. Through the observation of the samples, it is found that many dissolution holes and microcracks are developed in the shale, and the overall porosity is better developed, with large pore space and good connectivity, and a larger amount of pyrite can be seen; (3) The pore size of the marine shale of the Ordovician Wulalik Formation in the western Ordos Basin ranges from 1 to 45 μm, with 3 to 15 μm dominating, and the total pore volume of the shale is mainly provided by relatively small pores below 20 μm; (4) The poor connectivity of the study area may be due to the low thermal evolution of the shale in the study area and the limitation of micron CT accuracy.

Keywords: shale rock; Micron CT; Characterization of pore structure; Majiatan area.

1   Introduction

Porosity, pore type, and pore structure of gas-bearing shale affect the gas storage properties of the shale[1].Analyzing the structural types and developmental characteristics of nanoscale pores in gas-containing shales is of great significance in identifying the shale gas enrichment pattern and storage status[2].Currently, the challenge facing

China's major basins and oil and gas fields is how to develop low-permeability and ultra-low-permeability formations more efficiently, which also poses new requirements and challenges in terms of resource development and utilization. Unconventional oil and gas resources are gradually occupying an important position in the global energy structure due to their wide distribution and abundant reserves, so it is urgent to carry out in-depth research on unconventional oil and gas and realize exploration and development[3].

The Upper Ordovician Wulalik Formation is only developed in the western part of the Ordos Basin, and is the best set of hydrocarbon source rocks in the Lower Paleozoic. Since 2017, the Wulalik Formation has shown a new pattern of oil and gas exploration in parallel and in full bloom, confirming its good exploration potential[4].

This paper takes the Ordos Basin western Ordovician Wulalik Formation shale as the research object, and qualitatively and semi-quantitatively describes the shale pore type, morphology and pore scale by scanning electron microscope, and jointly characterizes the pore size distribution, pore morphology and pore structure of the reservoir with micrometer CT, and explores the controlling factors of the pore development in order to recognize the shale gas storage law of this area, and to provide a reference for the evaluation of the sea-phase shale gas exploration in the northern part of China. The results are summarized in the following table.

2   Geological Setting

The Ordos Basin is a vast area, starting from Yinshan Mountain and Daqing Mountain in the north, reaching the Qinling Mountains in the south, Liupanshan-Helan Mountains in the west and Luliang Mountains and Taihang Mountains in the east. With an area of 250,000 square kilometers, it is the second largest basin in China, covering five provinces and autonomous regions of Shaanxi, Gansu, Ningxia, Shanxi and Inner Mongolia. The Ordos Basin has six primary tectonic units, which are the North Shaanxi Slope, the Yimeng Rise, the Weibei Rise, the Tianhuan Depression, the Western Marginal Rise Belt, and the Western Shanxi Flexure Belt, and the study area is located in the western margin of the basin, with the Qilian orogenic belt in the south and the Alxa Massif in the north, which has frequent tectonic activities, and contains two tectonic units, namely the Tianhuan Depression and the Western Marginal Flexure Belt. The Ordos Basin is a multi-rotation Craton basin with stable subsidence, depression migration and obvious torsion, which is characterized by inhomogeneous nature of the basement and undulating bedrock top surface, but the cover structure is simple, which contains rich hydrocarbon resources.

The depositional pattern of the Wulalik Formation is "three-stage", with two sets of mud shale at the top and bottom, and a section of limestone in the middle. The thickness of mud shale at the bottom is 25-60m, dominated by mud shale with high mud content; the thickness of mud shale at the top is 45-55m, dominated by gray mudstone and mud shale; the total thickness of mud shale ranges from 25 to 115m; the development in plan view is relatively stable, the abundance of organic matter is not high on the whole, and the value of TOC is 0.30%-1.15%; the kerogen is dominated by Type I, with a small

amount of Type II$_1$, and it has generally reached the mature and high-mature stage, and some of them have reached the over-mature stage. The cheese root is mainly of type I, with a small amount of type II$_1$, generally reaching the stage of high maturity, and some of them reaching the stage of over-maturity, with good conditions for gas production. Limestone generally consists of 2 sections of lithologically pure marl-bearing limestone and marl, with a thickness of 0 to 27 m. The thickness gradually decreases from south to north in the plane, from 2 sections to 1 section until it is not developed[5].

3   Materials and Methods

The pore structure of Wulalik Formation in the western Ordos Basin was analyzed by field emission scanning electron microscopy (SEM) and micron CT to observe the pore type, size, quantity and the degree of fracture development[6][7]. The SUPRA 55 field emission scanning electron microscope was used. The instrument used for micron CT is the Carl Zeiss Xradia 510 Versa, which has a maximum resolution of 0.7μm.

   CT scanning technology allows the scanning of specific sections of an object and the resulting series of two-dimensional images can be reduced to a three-dimensional model through the use of software[8]. Imaging with micron CT is based on density differences, using grayscale to distinguish between different components of the sample. Among them, the high-density component shows bright white (e.g., pyrite), the medium-density component shows light gray (e.g., quartz, carbonate minerals, clay minerals), the low-density component shows dark gray (e.g., organic matter), and the pores (cracks) are black [9][10].Two samples were selected for this experiment, ZHP-1-4245.92 and ZHP-1-4246.92.

4   Characterization of Reservoir Pore Structure

4.1   Pore Types

Scanning electron microscopy can clearly identify and classify the pores of the Wulalik Shale samples, thus qualitatively characterizing the pores of the samples. Through field emission scanning electron microscopy observation of 22 samples, it is found that the mud shale of the Wulalik Formation in the study area is very dense and mainly develops nanometer-sized pores, and the types of pores include four categories: intergranular pores (intergranular pores), interlayer slits of clay minerals, dissolution pores, and organic matter pores. In addition to matrix porosity, microfractures and cracks are also more developed.

   (1) Intergranular pores (intergranular pores). This type of pore is formed in the brittle debris particles or formed in the pyrite crystals and not filled with organic matter and clay irregular pores, pore size, connectivity is good, is the main place of free gas storage[11].

   (2) Clay mineral interlayer fracture. Slit-like intergranular pores formed as a result of bending of plastic clay minerals due to brittle minerals blocking their continued compaction[6]. The pore morphology of the interlayer seams of clay minerals is mostly flat,

elongated and often filled with organic matter. The mechanism of this pore formation is that when compaction is gradually increased, the clay minerals undergo dewatering and interlayer joints appear[12], It can also be formed due to the transformation of montmorillonite to ilmenite and illite during diagenesis and the reduction in the volume of clay minerals, which have good seepage capacity and strong adsorption, and are the main places for adsorption gas storage[11].

(3) Dissolution pores (Figure 1, b, e, g). These pores are mostly intra-granular pores formed within carbonate particles due to dissolution and erosion, with small pore size and poor connectivity, contributing less to shale gas adsorption and storage, and the carbonate rock content in the study area is high, with a larger proportion of dissolution pores.

(4) Organic pores are pores developed in organic matter, most of which are very small and are intra-granular pores. Organic pores are not common in shale reservoirs in the study area, which is related to the low abundance and evolution of organic matter in the study area[11].
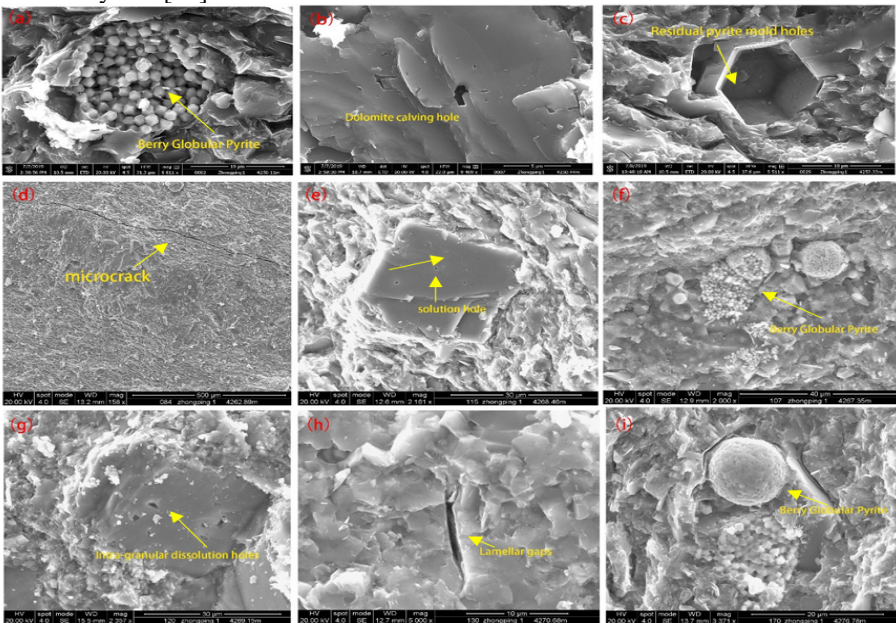
Fig. 1. (a) Berry-globular pyrite, ZP1 well, 4250.11m; (b) dolomite dissolution holes, ZP1 well, 4250.44m; (c) a few residual pyrite cast holes and dissolution holes, where iron dolomite is seen to fill in, ZP1 well, 4253.33m; (d) microfractures, ZP1 well, 4262.89m; (e) dissolution holes, ZP1 well 4268.46m; (f) berry-globular pyrite, ZP1 well, 4267.35m; (g) intra-granular dissolution holes, ZP1 well, 4269.15m; (h) lamellar crevices, ZP1 well, 4270.68m; (i) berry-globular pyrite, ZP1 well, 4276.78m

Through the observation of the samples, it is found that the shale is mostly developed with dissolution pore holes and microcracks, the overall pore development is good, the pore space is large and well connected, and more pyrite is seen.

4.2   Micron CT

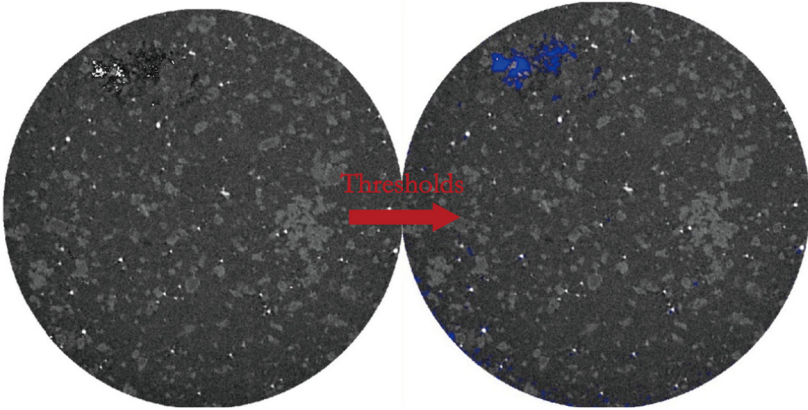### 4.2.1 Pore Structure Extraction.

Fig. 2. 2D slice map to extract pores

According to the different gray levels of different substances, the pores in the samples were extracted by threshold division (as shown in the blue area in the upper right panel of Figure 2), and the percentage of the volume of the study area occupied by the pores (i.e., porosity) of ZHP-1-4245.92 was 0.02%, with a pore volume of 43,109.027 µm³, a pore surface area of 53,421.3929 µm2, and a rock specific surface of 1.24 µm2/µm³. The percentage of volume of the study area occupied by pores (i.e., porosity) of ZHP-1-4246.92 is 0.33%, with a pore volume of 884,309.8925 µm³, a pore surface area of 1184,762.57 µm2, and a rock specific surface of 1.34 µm2/µm³.The spatial distribution of the pores of the two samples can be demonstrated by CT data processing (Figure 3).
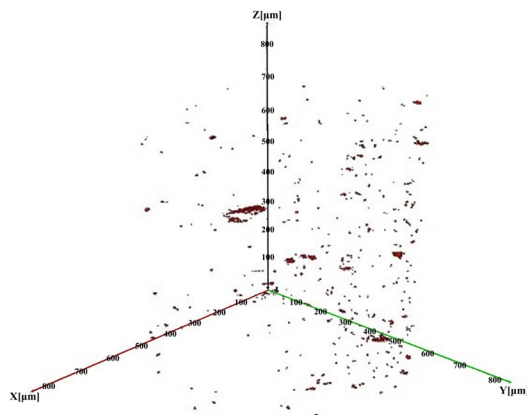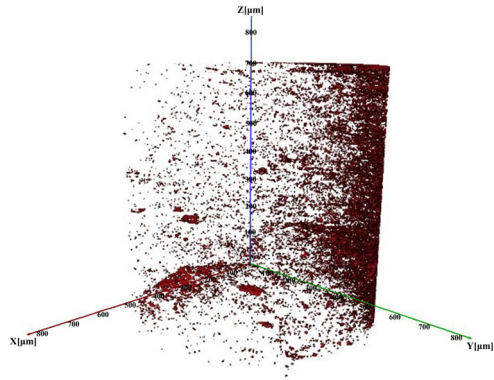
Fig. 3. Three-dimensional display of ZHP-1-4245.92 and ZHP-1-4246.92 pores

4.2.2 Layer-by-Layer Porosity.

x axis   y axis   z axis
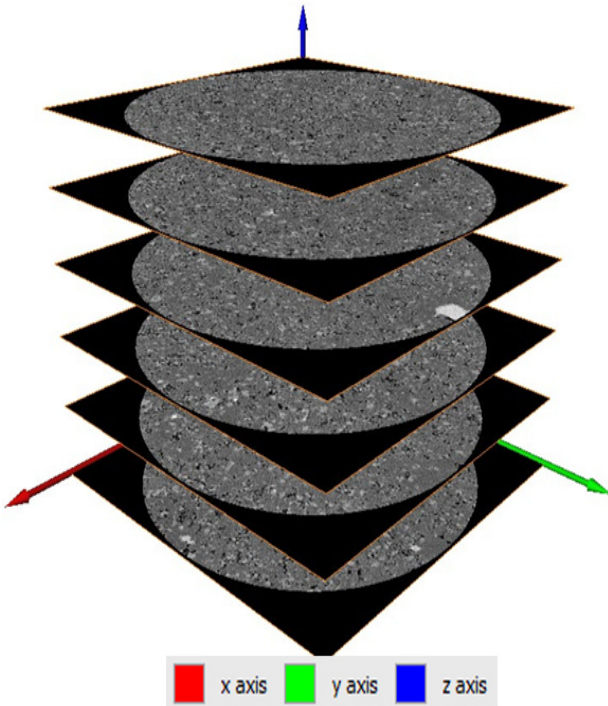
Fig. 4. Example of principles for defining layer-by-layer face porosity

$Level - by - level\ porosity\ in\ the\ Z - axis\ direction$
$$= \frac{Layer - by - layer\ pore\ area\ in\ the\ Z - axis\ direction}{Level - by - level\ area}$$
$\times 100\%$
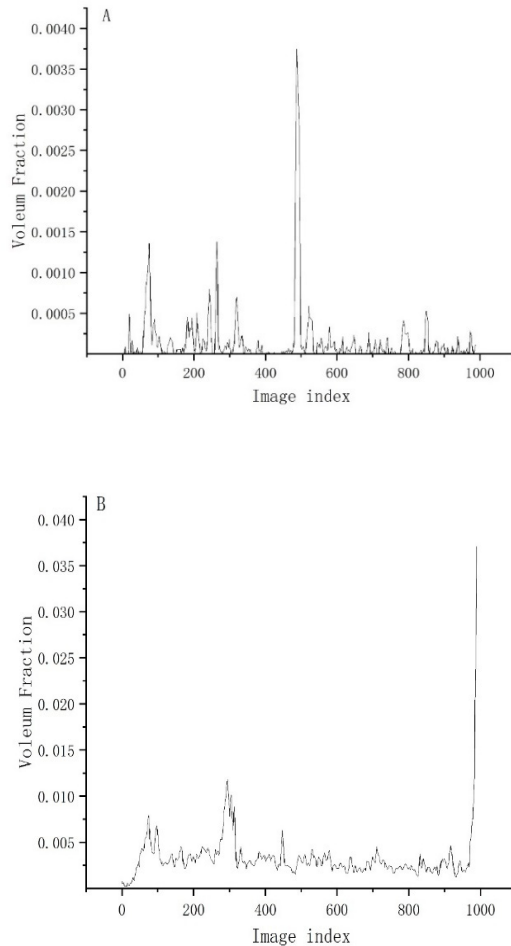
Fig. 5. Layer-by-Layer Porosity Changes for ZHP-1-4245.92 and ZHP-1-4246.92

The layer-by-layer porosity of the sample can be obtained by calculating the porosity of each layer separately (Figure 4). From the level-by-level porosity analysis in the Z direction, it can be seen that the overall fluctuation is very large, and the average surface porosity of ZHP-1-4245.92 is 6.88765×10-5 and the average surface porosity of ZHP-1-4246.92 is 0.29% (Figure 5).

4.2.3 Pore Marking and Sieve Statistics.
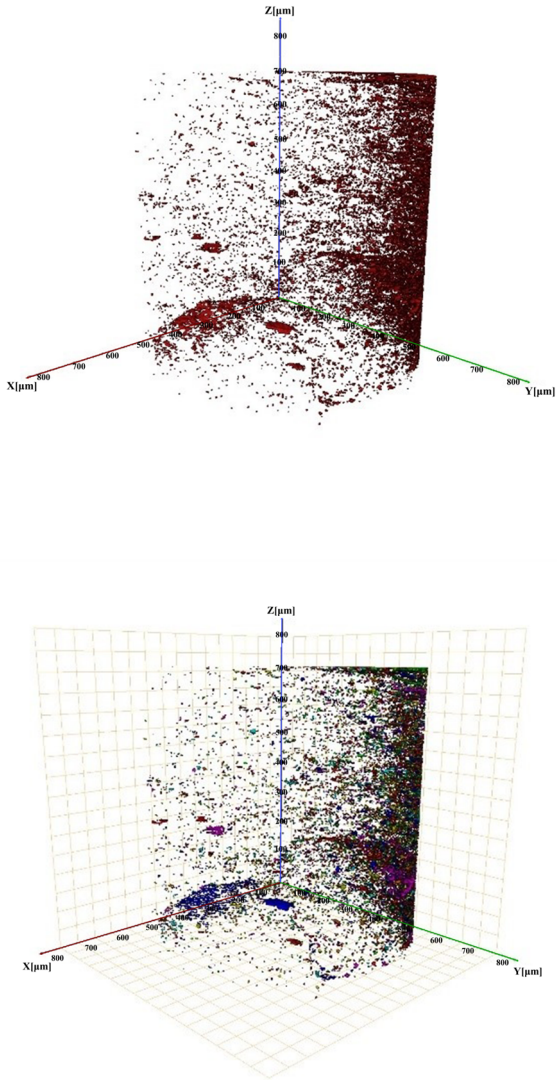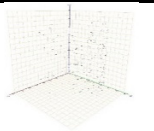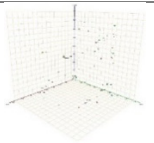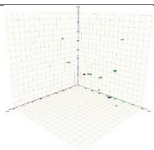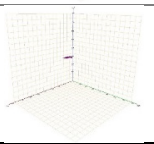
Fig. 6. Labeling and sieving statistics for pore structure

   The extracted pores were marked with different colors showing individual isolated pores, and the pores were sieved and counted according to their volume size(Figure 6). The experimental results are shown in Tables 1 and 2:

Table 1. Statistics of ZHP-1-4245.92 experimental results

Pore volume range	Number (pcs)	Number as a percentage of total pore number	Pore volume (µm³)	Pore area (µm2)	Percentage of total pore volume	
EqD≤5um	296	76.29%	9798.88	16253.6	22.73%	
5um<EqD≤10um	79	20.36%	12365.3	15623.3	28.68%	
10um<EqD≤15um	12	3.10%	11939.09	12322.54	27.70%	
25um<EqD≤30um	1	0.26%	9005.73	9221.99	20.89	
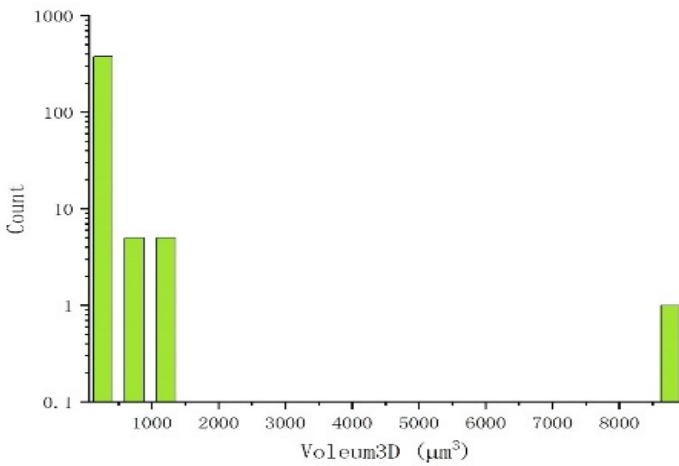
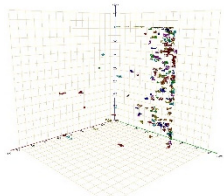**Fig. 7.** Pore volume distribution
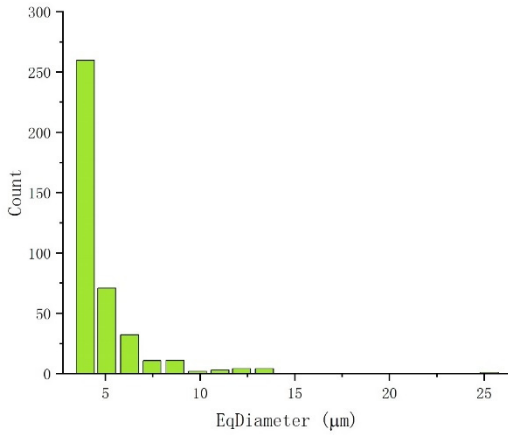
Fig. 8. Equivalent diameter distribution of pores

The pore volume and pore equivalent diameter distributions of ZHP-1-4245.92 are shown in Figures 7 and 8. The results show that the pore size of ZHP-1-4245.92 is mainly distributed below 1500 μm3, and the equivalent diameter of the pores is mainly distributed in the range of 5-14 μm and 25 μm. This is consistent with the results obtained from 3D simulation.

Table 2. Statistics of ZHP-1-4246.92 experimental results

Pore volume range	Number (pcs)	Number as a percentage of total pore number	Pore volume (μm³)	Pore area (μm2)	Percentage of total pore volume	
EqD≤10 um	11554	98.55%	466768	724087	52.78%	
10um<EqD≤20um	154	1.31%	169082	189740	19.12%	

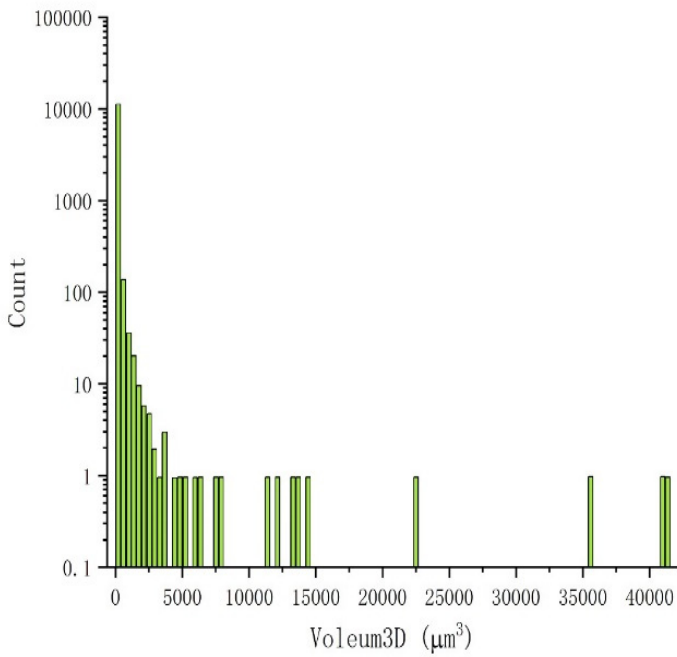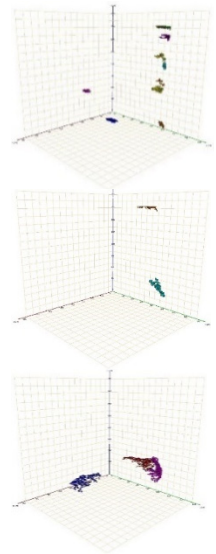|						
20um<EqD≤30um	11	0.09%	93502	91881.3	10.57%	
30um<EqD≤40um	2	0.02%	36983.5	39534.2	4.18%	
40um<EqD≤50um	3	0.03%	117974	139520	13.34%	

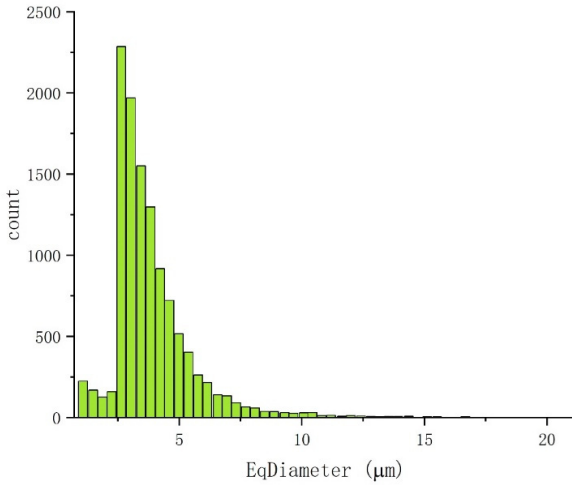**Fig. 9.** Pore volume distribution

Fig. 10. Equivalent diameter distribution of pores

The pore volume and pore equivalent diameter distributions of ZHP-1-4246.92 are shown in Figures 9 and 10. The results show that the pore size of ZHP-1-4246.92 is mainly distributed below 6000 μm3, while the pore equivalent diameter is mainly distributed below 20 μm. The pore size and equivalent radius are significantly stronger than the other sample.

4.2.4 Extraction of Organic Matter and Minerals.
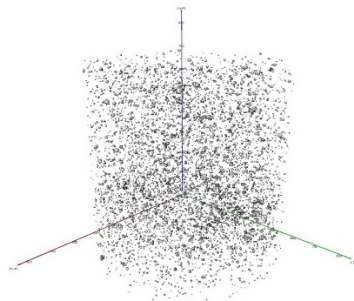ZHP-1-4245.92:

Fig. 11. Extraction of Minerals

The spatial distribution of minerals and organic matter in the samples can be obtained by processing the CT data (Figure 11). Based on the extracted data, 0.16% of minerals were available and no organic matter was found.
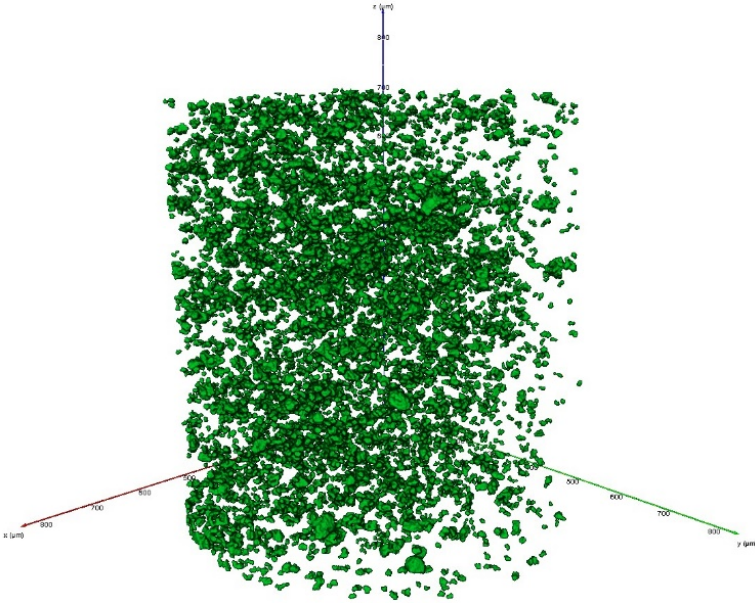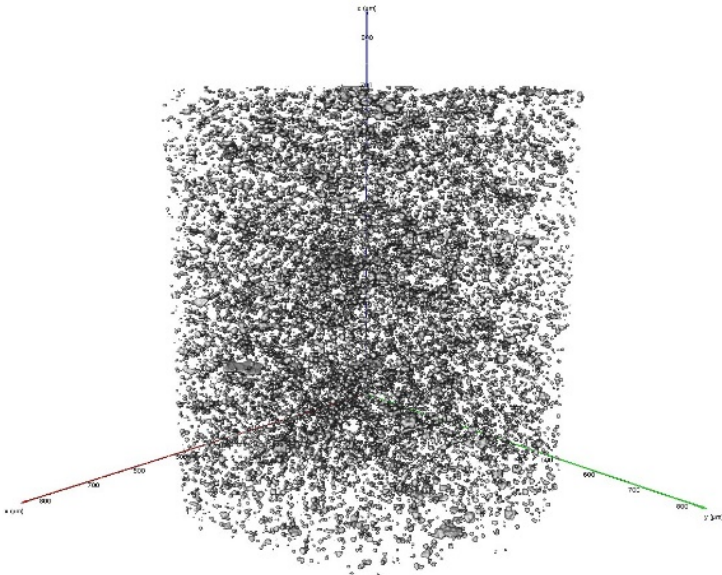ZHP-1-4246.92:

Fig. 12. Extraction of organic matter

Fig. 13. Extraction of minerals

The spatial distribution of minerals and organic matter in this sample is shown in Figures 12 and 13. Based on the extracted data, it can be concluded that the proportion of organic matter is 1.34% of the total volume and 0.8% of minerals.
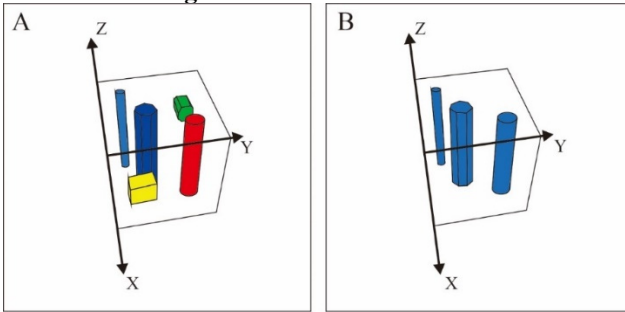
4.2.5 Extraction of Connecting Holes.

Fig. 14. Example of Defining Principles for Connected and Disconnected Holes

A pore that connects two faces in a bounding box is a connected pore, and the opposite is a disconnected pore. Figure 14 illustrates the defining principles for software to determine whether or not it is connected.

At a resolution of 0.7203 μm, both samples were free of connected pores.

5   Disscussion

5.1   Porosity Evaluation

In the Ordos Basin Western Ordovician Wulalik Formation shale, the porosity measured by helium method is lower than 4.00% in general, mainly from 0.16% to 1.50%, with the minimum value of 0.08%, the maximum of 4.20%, and the average of 1.20%, and the porosity greater than 4.00% accounts for a small percentage[11]. Micron CT analysis yielded porosities of 0.02% and 0.33%, which are smaller than those measured by helium. CT-reduced 3D cores show that no cracks were seen in the samples. This is because the CT samples avoided the cracks in the rock samples, making the porosity obtained from CT lower. At the same time, the poor resolving power of micrometer CT prevents any pores and slits smaller than 0.7203 μm from being characterized, so the measured porosity is low.

5.2   Pore Characterization and its Connectivity Analysis

Micron CT showed that the number of pores with pore sizes smaller than 20 μm was high and accounted for a large portion of the total pores. The main reasons for this are: (1) the shale is denser and has no cracks in the samples, so the measurable pores are smaller; (2) pores with a pore size larger than 1 μm are mainly larger dissolution pores or microfractures, which can provide a larger pore volume[13].

The connectivity of the pores of the shale samples measured by micrometer CT is poor. The pores in the southern shale reservoirs are mainly organic pores[14][15], which are related to the high maturity of shale development. The study area is less mature than the southern shale, and the organic pores are developed within (or at the

edges) of the organic matter and are better connected to each other, however, because the pore size is generally less than 500 nm, it is difficult to distinguish them with the precision of this experiment. Therefore, micrometer CT did not yield good connectivity.

6 Conclusions

(1) The marine shale of Ordos Basin Western Ordovician Wulalik Formation is more developed in overall porosity, through the observation of the samples, it is found that the shale mostly develops dissolution holes and microcracks, and the overall porosity is better developed, the pore space is large and better connected, and more pyrite can be seen.

(2) The analytical results of micrometer CT show that the pore size of the marine shale of the Ordovician Wulalik Formation in the western Ordos Basin ranges from 1 to 45 μm, with a predominance of 3 to 15 μm. Based on the full-size pore distribution of the shale, it is recognized that the total pore volume of the shale is mainly provided by relatively small pores below 20 μm.

(3) Poor connectivity in the study area may be due to the low thermal evolution of the shale in the study area and the limitations of micrometer CT accuracy.

Data Availability

Data is provided within the manuscript or supplementary information files

Author Contributions Statement

Wenyi Sun conceptualized and designed the research, conducted sampling and experiments, and wrote the first draft. Wenyi Sun and Xi Li contributed to the results and discussions. All authors revised and approved the manuscript. All authors reviewed the manuscript.

Funding

Competing interests

The authors declare no competing interests.

References

1. Zou, C.; Zhu, R.; Bai, B.; Yang, Z.; Wu, S.; Su, L.; Dong, D.; Li, X. (2011) First discovery of nano-pore throat in oil and gas reservoir in China and its scientific value. Acta Petrological Sinica , 27(6) :1857 - 1864.

2. Zhu, Y.; Wang, Y.; Chen, S.; Z, H.; Fu, C. (2016) Qualitative-quantitative multiscale characterization of pore structures in shale reservoirs : A case study of Longmaxi Formation in the Upper Yangtze area. Earth Science Frontiers, 23(1) :54-163.

3. Zhang, E. (2021) Study on Shale Reservoir Characteristics of Shanxi Formation in Yanchi Area, Ordos Basin. MA, China University of Geosciences (Beijing), Beijing.

4. Xi, S.; Liu, X.; H, Z.; Zhao, H.; Zhang, C.; Liu, Y. (2023) Enrichment characteristics and exploration direction of shale oil and gas in Wulalike Formation of Middle Ordovician in the Ordos Basin. Natural Gas Industry, 43(3): 12-22.

5. Wu, D.; Wu, X.; Li, C.; Yu, Z.; Li, W.; Cai, J.; Li, G. (2021) Sedimentary model and hydrocarbon-generation potential of source rock of the Ordovician Ulalik Formation in western Ordos Basin. Marine Hydrocarbon Geology, 26(2): 123-130.

6. Curtis, M.E.; Sondergeld, C.H.; Ambrose, R.J.; Rai, C.S. (2012)Microstructural investigation of gas shales in two and three dimensions using nanometer-scale resolution imaging. AAPG bulletin, 96(4), 665-677..

7. Ji, W.; Song, Y.; Jiang, Z.; Chen, L.; W, P.; Liu, Q.; Gao, F.; Yang, X. (2016) Micro-nano pore structure characteristics and its control factors of shale in Longmaxi Formation, southeastern Sichuan Basin. Acta Petrolei Sinica, 37(2): 182.

8. Sondergeld, C.H.; Ambrose, R.J.; Rai, C.S.; Moncrieff, J. (2010) Micro-structural studies of gas shales. In SPE Unconventional Resources Conference/Gas Technology Symposium . Pittsburgh, Pennsylvania, USA. pp. SPE-131771.

9. Guo, X.; He, S.; Chen, S.; Chen, X.; Wang, S.; Qin, L. (2016) Research on Microstructure of Shale Pores and Distribution Features Based on Nano-CT Scanning and Digital Core Analysis. Coal Geology of China, 28(2): 28-34.

10. Wu, S.; Zhu, R.; Cui, J.; Bai, B; Zhang, X.; Jin, Xu.; Zhu, D.; You, J.; Li, X. (2015) Characteristics of lacustrine shale porosity evolution, Triassic Chang 7 Member, Ordos Basin, NW China. Petroleum Exploration and Development, 42(2): 167-176.

11. Zhang, F.; Li, Y.; Luo, J.; Ren, X.; Zhang, L.; Zhang, J. (2022) Microscopic pore structure characteristics of shale of Ordovician Wulalike Formation in western Ordos Basin. Lithologic Reservoirs,34(5):50-62.

12. Zheng, S.; Liu, L.; Wang, Y.; Luo, Z.; Wang, X.; Sheng, Y.; Xu, T.; Wang, B. (2019) Characteristics of microscopic pore structures and main controlling factors of Wufeng-Longmaxi Formation shale in southern Sichuan Basin. Lithologic Reservoirs,31(3):55-65.

13. Zhao, J.; Yao, J.; Zhang, L.; Yang, Y.; Sun, H.; Sun, Z.; Bai, Y. (2018) Effects of microfractures on gas flow in tight porous media. Journal of China University of Petroleum, 42(1): 90-98.

14. Jiang, Z.; Tang, X.; Li, Z.; Huang, H.; Yang, P.; Yang, X.; Li, W.; Hao, J. (2016) The whole aperture pore structure characteristics and its effect on gas content of the Longmaxi Formation shale in the southeastern Sichuan basin. Earth Science Frontiers,23(2):126-134.

15. Ma, Z.; Zheng, L.; Xu, X.; Bao, F.; Yu, X. (2017) Thermal simulation experiment on the formation and evolution of organic pores in organic rich shale. Acta Petrolei Sinica, 38(1): 23.